

pubs.acs.org/cm Article

Pd-Au Asymmetric Nanopyramids: Lateral vs Vertical Growth of Au on Pd Decahedral Seeds

Li Zhou, Xiaoyu Qiu, Zhiheng Lyu, Ming Zhao, and Younan Xia*



Cite This: https://doi.org/10.1021/acs.chemmater.1c01489



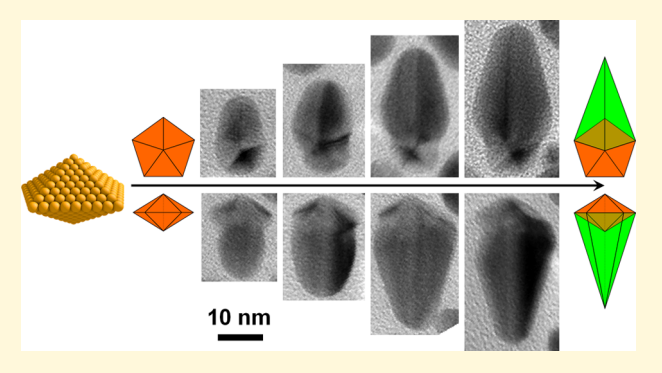
ACCESS

III Metrics & More

Article Recommendations

SI Supporting Information

ABSTRACT: Seed-mediated growth in a site-selected and asymmetric fashion provides a versatile route to the fabrication of noblemetal nanocrystals with unique optical and catalytic properties. Herein, we report the synthesis of Pd—Au asymmetric nanopyramids through the site-selected growth of Au from penta-twinned Pd decahedral seeds. As a result of symmetry breaking arising from slow reduction kinetics, we observed two asymmetric growth modes: lateral growth initiated from one of the five edge vertices along the twin boundary and vertical growth from one of the two axial vertices along the fivefold axis, with the former being more favorable. The slow reduction kinetics was achieved by switching from $AuCl_4^-$ to $AuBr_4^-$ as a precursor, together with the use of L-ascorbic acid 2-



phosphate trisodium salt (Asc-2P) for its relatively weaker reduction power than ascorbic acid. The aspect ratio and tip sharpness of the nanopyramids could be manipulated by varying the amount of Ag⁺ ions introduced into the growth solution. The nanopyramids exhibited two surface plasmon resonance peaks, corresponding to the transverse and longitudinal modes, and the extinction spectra could be used to track the growth and evolution of morphology. This work not only enriches our understanding of seed-mediated growth on multiply-twinned decahedra but also provides an effective strategy for preparing bimetallic nanocrystals with asymmetric morphology and tapered dimensions for the creation of high-index facets on the surface.

■ INTRODUCTION

Noble-metal nanocrystals with anisotropic morphology have attracted intense attention due to the unique properties different from their spherical counterparts. 1-3 For Au nanorods, the one-dimensional, anisotropic morphology gives them two typical extinction peaks corresponding to the transverse and longitudinal modes of surface plasmon resonance.^{4,5} In addition to the dual peaks of plasmon resonance, Au bipyramids possess stronger local field enhancement at the sharp corners than that at the rounded ends of nanorods. Since noble metals have a face-centered cubic (fcc) lattice, symmetry breaking is needed for the preparation of anisotropic morphology.8 Over the past two decades, remarkable progress has been made in the anisotropic growth of noble-meal nanocrystals through the achievement of an understanding of the explicit roles played by capping agents, 9,10 twin defects, 11 stacking faults, 12 and reaction kinetics. 13

Compared to their single-crystal counterpart, nanocrystals with twin defects provide more opportunities for tailoring the morphology. Taking decahedron as an example, it is enclosed by the 10 {111} facets and can be considered as an assembly of five tetrahedral units by sharing five {111}-twin planes (Figure S1a). When applied to seed-mediated growth, many distinctive morphologies can be obtained by controlling the deposition of the same or a different metal on the surface of a decahedral seed. Specifically, the low coordination number of

the vertices, the twin defects intersecting the vertices and ridges, and the square packing of the {100} facets on the edges can all play important roles in determining the final morphology. In the case of symmetric growth, our group reported the synthesis of Pd@Pt core-shell decahedra by depositing a few layers of Pt atoms on Pd decahedral seeds. The Pt atoms preferred to stay at the vertices, ridges, and edges of a decahedron for the generation of a concave morphology. 15 Interestingly, a core-frame structure was also reported by leveraging the difference in surface free energy between the vertices, edges, and ridges, as well as the {111} facets. To this end, Kitaev and co-workers selectively deposited ultrathin Au nanoframes with a thickness of 1.6-5 nm on the edges and ridges of Ag decahedral seeds by controlling the amount of the deposited Au under optimized reduction conditions. 16 Huang and co-workers reported a similar core-frame structure through edge-selected etching of Au decahedra and subsequent deposition of Pt on the sites high in surface free energy and

Received: April 29, 2021 Revised: June 8, 2021



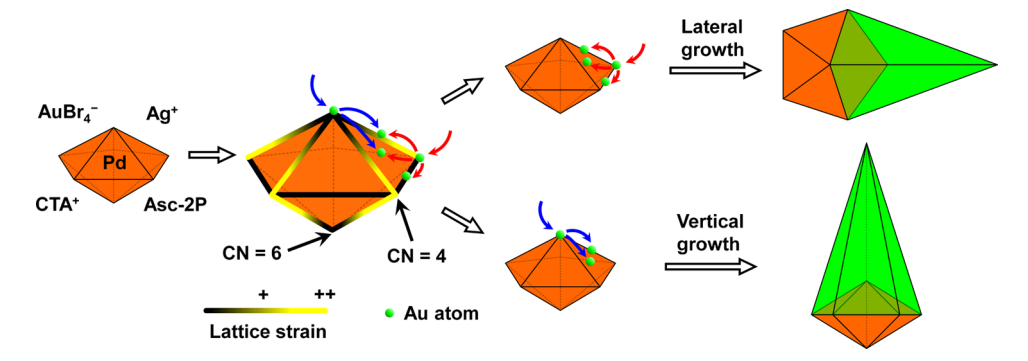


Figure 1. Schematic illustration of the lateral and vertical modes involved in the growth of Au on Pd decahedral seeds. The deposition is initialed from the vertices due to the large curvature, small coordination number (CN), and great lattice strain. The site-selected and asymmetric growth leads to the formation of nanopyramids with a sharpened tip.

located at the ridges and the etched edges, and a ring-like Pt nanostructure was obtained after the complete removal of Au by etching.¹⁷

Anisotropic morphologies such as nanorods, nanowires, bipyramids, and multiple-armed stars can also be synthesized by depositing the same or a different metal on the surface of decahedral seeds. One-dimensional nanocrystals (e.g., nanorods, nanowires, or bipyramids) involving vertical growth along the fivefold axis of decahedra, that is, the $\langle 110 \rangle$ direction, is a representative anisotropic growth mode. Such growth is assisted by the selective adsorption of capping agents on the {100} side faces 18,19 or driven by the crystallographic structure with the atom deposition being initiated at the high-surfaceenergy ridges^{20–22} and by restraining the radial growth that has gradually increased the lattice strain at twin boundaries. 23,2 The commonly reported synthesis of Au, Ag, Cu, Pt, and Pd nanorods, nanowires, and bipyramids with a penta-twinned structure using a one-pot method are typically believed to involve the nucleation of decahedral seeds, followed by the subsequent anisotropic atom deposition on the seeds. 18,25-30 Along the same line, seed-mediated growth of one-dimensional metal nanocrystals^{31–36} has also been reported for well-defined decahedral seeds prepared in advance. When the same metal was involved, Kitaev and co-workers reported the growth of Ag nanorods from Ag decahedral seeds with precise control over both the length and width. ^{20–22} Using a light-induced method, Mirkin and co-workers applied low-energy excitation wavelengths between 600 and 750 nm to control the reaction rate and thus the aspect ratio of Ag nanorods growing from 7.9-nm Ag decahedral seeds.³⁷ Huang and co-workers reported the growth of Au bipyramid and nanorods by employing Au decahedral seeds with different sizes in the range of 25-49 nm. 38,39 Our group reported the growth of Pd nanorods from Pd decahedral seeds, as well as tapered Pd nanorods when the system was subjected to oxidative etching by $O_2/I^{-0.40,41}$

In principle, the vertical growth could occur on both sides of the decahedral seed, or just one of them for the involvement of asymmetric growth. When the growth involves the same metal as that in the seed, it is impossible to differentiate the symmetric and asymmetric growth modes. When different metals are involved, however, the symmetry of vertical growth can be easily resolved. To this end, symmetric growth on Au decahedral seeds was reported for the synthesis of Ag—Au—Ag and Pd—Au—Pd nanorods, with the Au seeds situated at the middle point. ^{42,43} On the other hand, our group reported the synthesis of Ag—Pd and Cu—Pd nanorods through asymmetric growth only from one side of the Pd decahedral seeds, and the

symmetry breaking was attributed to the slow reaction kinetics and a relatively large lattice mismatch between the two metals.44-46 The symmetry of vertical growth was also explicitly manipulated by varying the reaction kinetics. By simply adjusting the pH value of the solution, Mirkin and coworkers reported the light-induced overgrowth of Ag on Au decahedral seeds for the synthesis of symmetric Ag-Au-Ag nanorods, as well as the asymmetric Au-Ag icosahedra. Similarly, by adjusting the reaction rate through the addition of aqueous ammonia, Huang and co-workers reported both symmetric and asymmetric growth of Ag nanorods on Au decahedral seeds. 48 Besides the aforementioned vertical growth mode, in-plane, lateral growth along the radial direction or the twin boundaries (the (211) direction) of a decahedron was also developed to synthesize multiple-armed nanocrystals, especially symmetric, pentagram-shaped stars. 49-52 The pentagram-shaped stars were also synthesized through lateral growth along the (100) directions of the five single-crystal subunits. 53,54 In addition, there are reports on highly branched nanocrystals growing simultaneously along the two vertical (110) directions and the five lateral (211) directions. 55,56 However, compared with the symmetric morphology, asymmetric nanocrystals growing from decahedral seeds are seldom reported (except for the vertically grown Pd-Ag nanorods, 44,45 Pd-Cu nanorods, 46 Au-Ag nanorods, 48 and Au-Ag icosahedra⁴⁷) and the underlying growth mechanism still needs to be elucidated.

Herein, we report the synthesis of Pd-Au asymmetric nanopyramids through site-selected growth of Au on Pd decahedral seeds. Interestingly, we observed asymmetric growth along both lateral (initiated from one of the edge vertices) and vertical (initiated from one of the axial vertices) directions. We systematically examined the effects of experimental conditions on the growth process. Several factors were found to be instrumental to the achievement of siteselected and asymmetric growth. First, the initial growth positions are located at the axial and edge vertices due to their higher surface free energies arising from the lower atomic coordination number and higher lattice strain. Second, asymmetric growth can be achieved through the formation of AuBr₄ precursor, which is harder to reduce relative to AuCl₄-,⁵⁷ and the use of a reducing agent such as L-ascorbic acid 2-phosphate trisodium salt (Asc-2P) with a lower reduction power compared with the commonly used ascorbic acid (AA). Finally, the relatively large (4.8%) lattice mismatch between Au and Pd also contributes to the asymmetric growth. The mechanistic understanding from this

work offers a great opportunity for achieving the controlled growth of nanocrystals with asymmetric morphology.

RESULTS AND DISCUSSION

The penta-twinned Pd decahedral seeds used to direct the growth of Au were prepared using a protocol developed in our group. 59,60 Figure S2a shows a typical transmission electron microscopic (TEM) image of the seeds. The growth of Au was conducted at 37 °C in a mixture containing HAuCl₄, AgNO₃, and hexadecyltrimethylammonium bromide (CTAB), together with the use of Asc-2P as a reducing agent in the presence of Pd decahedral seeds. The mixing of AuCl₄ with CTAB immediately resulted in the formation of a more stable complex of AuBr₄⁻ to give a deep brown color to the aqueous solution. This new precursor complex is harder to reduce relative to AuCl₄-, as reflected by their standard reduction potentials: 0.85 vs 1.00 V for the AuBr₄⁻/Au and AuCl₄⁻/Au pairs, respectively. 61 It should be pointed out that Asc-2P has a relatively lower reducing power than AA,58 a two-electron reductant more commonly used in the colloidal synthesis of metal nanocrystals (Figure S3). As soon as Asc-2P was introduced, the reaction solution turned colorless due to the reduction reaction of $AuBr_4^- + 2e^- \rightarrow AuBr_2^- + 2Br_2^{-.62}$ Subsequently, AuBr₂⁻ was reduced over a period of 3 h, with the resultant Au atoms nucleating and growing on the Pd decahedral seeds. The slow, two-step reduction of the Au(III) precursor made a major contribution to the asymmetric growth of the Pd-Au nanocrystals.44

As shown in Figure 1, the seven high-curvature vertices of a decahedron can be divided into two groups: (i) two axial vertices with a coordination number of 6 and (ii) five edge vertices with a coordination number of 4 and a tensile lattice strain (Figure S1a). The low coordination number and tensile strain make these vertices higher in surface free energy. As the reduction rate is slow, the surface reduction pathway should be in dominance due to its lower activation energy than that of the solution reduction pathway.⁶³ The high-curvature vertices with a higher surface free energy and higher electron density⁶⁴ would be more favorable for the heterogeneous nucleation or initial deposition of Au atoms. The final morphology of the Pd-Au nanocrystal will be determined by the relative kinetics involved in the deposition of atoms and the diffusion of adatoms to the neighboring ridges, edges, and {111} planes. 15 Assisted by the relatively large (4.8%) lattice mismatch between Au and Pd, the slow reduction rate would lead to asymmetric growth. Under this condition, the number of Au atoms would not be enough to initiate nucleation at every vertex on the decahedral seed, and subsequent growth of Au would preferentially occur at the sites already covered by Au due to the absence of lattice mismatch. Taken together, the growth of Au would be initiated from one of the vertices for the production of a Pd-Au asymmetric nanopyramid, corresponding to either lateral growth from an edge vertex or vertical growth from an axial vertex.

Figure 2a shows a TEM image of the as-prepared Pd—Au bimetallic nanocrystals. The nanocrystals exhibited the morphology of a pyramid, with a recognizable Pd seed at the base and a sharpened Au tip. Both the growth modes proposed in Figure 1 were observed in the products. To elucidate the growth mechanism, high-resolution high-angle annular dark-field scanning TEM (HAADF-STEM) imaging was performed to reveal the shape and internal structures of the Pd—Au nanopyramids. Figure 2b shows a typical HAADF-STEM

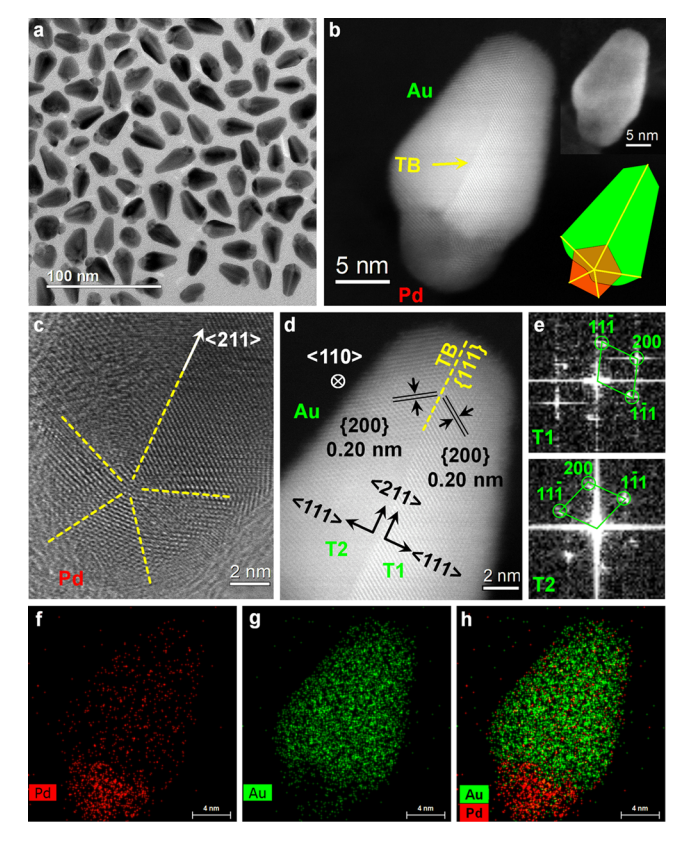


Figure 2. Structural and compositional analyses of the Pd—Au nanopyramids formed through lateral growth. (a) Typical TEM image of the Pd—Au nanopyramids. (b) HAADF-STEM image of an individual Pd—Au nanopyramid, where the Pd seed and Au pyramid can be easily distinguished due to their difference in contrast. A twin boundary (TB) in the Au region is also clearly observed. The insets show an SEM image and a schematic illustration. (c) Bright-field HRTEM image taken from the Pd domain. The five twin boundaries are marked by the yellow dashed lines. (d) Atomic-resolution HAADF-STEM image taken from the Au tip. (e) FFT patterns of the two subunits T1 and T2 in (d). (f—h) EDX mapping of an individual Pd—Au nanopyramid.

image of the Pd-Au nanopyramid corresponding to the lateral growth mode. The Pd and Au regions can be easily differentiated based on the imaging contrast. Figure 2c shows a bright-field HRTEM image focused on the region of the Pd decahedral seed, revealing the penta-twinned structure of an fcc lattice along the (110) axial direction. The Au was grown from a twin boundary along the (211) direction. A twin boundary was clearly observed in the Au region. The magnified image in Figure 2d shows the atomic structure of the Au tip, which was consistent with a twinned fcc lattice, with a {111} twin plane separating T1 and T2 subunits. The fringes with a lattice spacing of 0.20 nm corresponding to the {200} planes of Au were also observed in the T1 and T2 subunits. The fast Fourier transform (FFT) patterns for the T1 and T2 subunits (Figure 2e) were both consistent with the $\langle 110 \rangle$ zone axis and a shared {111} twin plane. The energy-dispersive X-ray spectroscopy (EDX) mapping images in Figure 2f-h clearly show the elemental distributions, confirming the overgrowth of Au from the Pd decahedral seed in an asymmetric fashion.

Figure 3 shows the case of asymmetric growth along the fivefold axis of a decahedral seed or the vertical $\langle 110 \rangle$ direction. Figure 3a shows the HAADF-STEM image of a vertically grown Pd-Au nanopyramid recorded in the

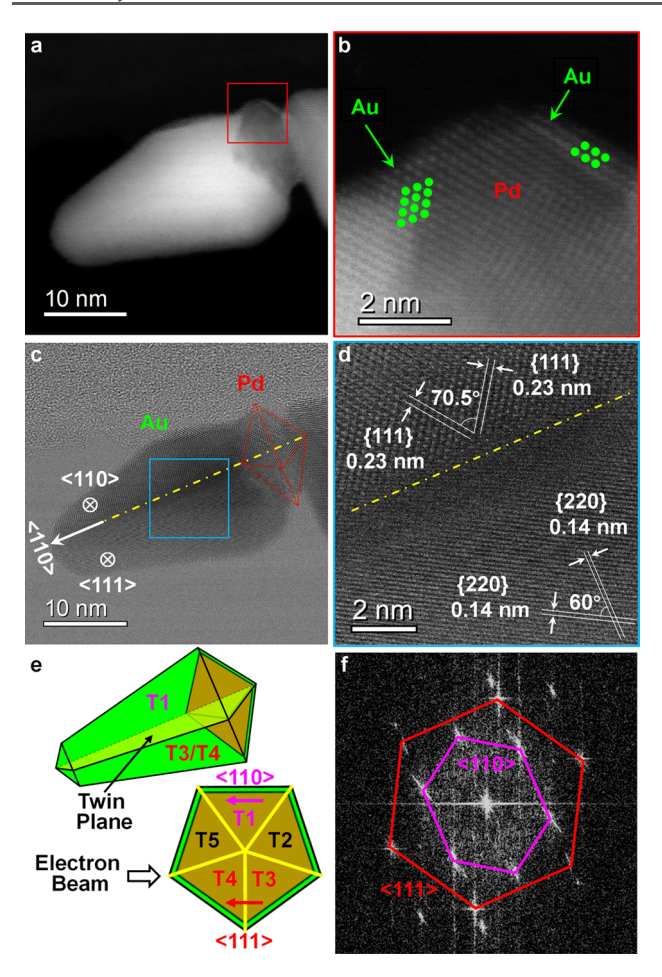


Figure 3. Structural and compositional analyses of the Pd–Au nanopyramids formed through vertical growth. (a) HAADF-STEM image of an individual Pd–Au nanopyramid. The diamond-shaped Pd seed and the Au pyramid can be clearly observed. (b) Atomic-resolution HAADF-STEM image taken from the red box in (a). Besides the growth of Au toward the left side along the 〈110〉 direction, a few atomic layers of Au are also found on the right side of the decahedral seed. (c) Bright-field HRTEM image of an individual Pd–Au nanopyramid. (d) Atomic-resolution HRTEM image taken from the blue box in (c). (e) Schematic illustrations of the right-side view and end-side view of the Pd–Au nanopyramid with five single-crystal subunits. (f) FFT pattern of the Au domain, showing a combination of the 〈111〉 and 〈110〉 zones.

direction perpendicular to the fivefold axis. The Pd decahedral seed shows a diamond shape (Figure S2b), together with a different contrast from Au. The Au pyramid is asymmetrically grown from one side of the Pd decahedral seed, while the other side is also covered by several atomic layers of Au (Figure 3b). We further analyzed the crystal lattice of the Au region to confirm the growth direction and the internal structure. As shown in Figure 3c, the red diamond shows the side view of a decahedron, while the yellow, dash-dotted line indicates the fivefold axis along the (110) direction. The magnified image in Figure 3d indicates that the vertically grown Pd-Au nanopyramid also has a typical penta-twinned structure. The crystal lattice of the upper part is consistent with the $\langle 110 \rangle$ zone with an interplane angle of 70.5° for the two {111} planes, while the bottom part exhibits the lattice fringe of the $\langle 111 \rangle$ zone with an interplane angle of 60° for the two $\{110/$ 220} planes. This result indicates that the projection direction is a combination of the $\langle 110 \rangle$ (T1 subunit) and $\langle 111 \rangle$ (T3/T4

subunit) zone axes, as shown by the schematic illustration in Figure 3e. The FFT pattern in Figure 3f corresponding to the Au region also shows a superposition of two fcc patterns from the $\langle 110 \rangle$ and $\langle 111 \rangle$ zones.

We also tracked the gradual growth of the Pd-Au nanopyramids. The Pd-Au nanocrystals obtained at t = 15min, 30 min, 1 h, and 2 h are shown in Figure 4a-d. An asymmetric heterodimer-type structure rather than a coreshell structure was observed at 15 min into the synthesis. With the increase of time, the Au domain gradually enlarged and a pyramidal shape was eventually obtained. Some obvious morphological or crystallography features could be observed and used to figure out the growth mode. As indicated by the blue arrows in Figure 4a, the penta-twinned pattern (Figure S2b) can be clearly observed in the Pd domains for some heterodimers; correspondingly, the twin boundary can be clearly seen as indicated by the red arrows in the Au domains, according to the lateral growth mode. As indicated by the green arrow, the diamond shape corresponds to the side view of a Pd decahedral seed, manifesting the vertical growth mode for this heterodimer. Several particles with different growth modes are singled out and shown in Figure 4e to demonstrate the typical morphologies of the Pd-Au nanopyramids at different reaction times. For the lateral growth mode, the penta-twinned pattern of the Pd seeds and the twin boundaries in the Au tips are obvious. In the case of the vertical growth mode, the diamond shape of the Pd seed from a side view is the characteristic feature.

The Pd-Au nanopyramids with obvious morphological or crystallography features (such as those indicated by the arrows in Figure 4a) can be assigned to the "ideal" cases of lateral and vertical growth modes proposed in Figure 1. However, for many particles lacking the above characteristics, some other features such as twin plane, tip angle, and orientation of the decahedral seed should be used to resolve the growth mode (Figure S4). Through a careful analysis of the Pd-Au nanopyramids in Figure 2a, the lateral and vertical growth modes account for about 56 and 36% of particles in the products. The higher percent of the lateral growth mode can be attributed to the fact that the edge vertex has the smallest coordination number in a decahedron while experiencing the greatest lattice strain, corresponding to the highest surface free energy. Meanwhile, there are five edge vertices per decahedral seed, whereas there are only two axial vertices. Although the underpotential deposition of Ag and the selective adsorption of the Ag-bromide complex or Br- on the {100} side faces could both promote vertical growth, ^{25,38,39} the lateral growth mode initiated from the edge vertex was more favorable than the vertical growth mode due to their differences in coordination number and lattice strain.

Since Au nanocrystals have characteristic surface plasmon resonances, the growth of Pd–Au nanocrystals with anisotropic morphology is clearly reflected in the time-elapsed extinction spectra recorded from the reaction mixture (Figure 4f). The extinction spectrum of the Pd–Au nanocrystals obtained at t=15 min exhibited a plasmon band around 540 nm, with a full width at half-maximum (FWHM) of 98 nm. With the increase of reaction time to 30 min, the plasmon band was greatly enhanced in intensity, while being slightly red-shifted to 550 nm and broadened to give an FWHM of 107 nm. As shown by the TEM images in Figure 4a,b, the plasmon bands of these two samples can be considered as a mixture of transverse and longitudinal modes of the anisotropic nano-

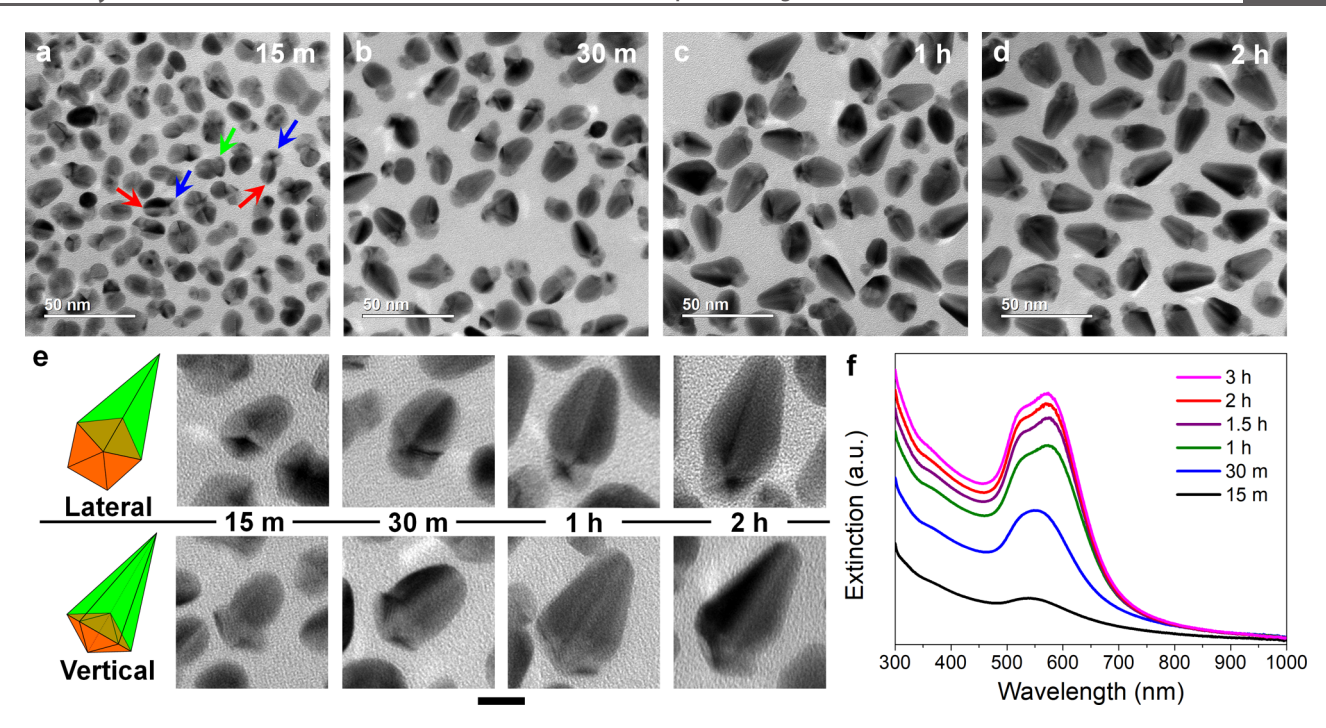


Figure 4. Time-dependent evolution of morphology and extinction spectra for the Pd–Au nanopyramids formed in a standard synthesis. (a–d) TEM images of the Pd–Au nanocrystals obtained at different time points: (a) 15 min, (b) 30 min, (c) 1 h, and (d) 2 h. The blue arrows indicate the Pd decahedral seeds with a clear penta-twinned pattern, and the red arrows indicate the corresponding twin boundary in the Au domains growing along the lateral direction. The green arrow indicates the diamond shape of the Pd decahedral seed (side view), implying the involvement of vertical growth for this heterodimer. (e) Typical morphologies of the Pd–Au nanopyramids obtained through lateral and vertical growth for different periods of time. The scale bar at the bottom is 10 nm. (f) Time-dependent evolution of the extinction spectra.

crystals. Since Pd has a larger imaginary dielectric constant than Au, the Pd-Au nanocrystals tend to suffer from greater plasmon damping than the counterparts made of pure Au, leading to reduced intensity and broadened width for the plasmon resonances.⁶⁵ Meanwhile, due to a small aspect ratio and a relatively broad size distribution, these two modes were not separated from each other, while the band shifting and broadening clearly indicate the increase in aspect ratio. As the synthesis proceeded to t = 1 h, the extinction spectrum showed further increase in intensity, exhibiting a main peak at 575 nm and a shoulder peak at 530 nm, corresponding to the longitudinal and transverse modes, respectively. The splitting of the extinction peaks indicates a further increase in aspect ratio. When the reaction time was further prolonged, the dual plasmon peaks slowly increased in intensity, while the peak positions remained almost unchanged, indicating that the Au growth rate slowed down and the aspect ratio was almost unchanged after t = 1.5 h.

We found that the presence of Ag⁺ ions was critical to the anisotropic growth and the concentration of AgNO₃ affected the final morphology of the Pd–Au nanopyramids. The presence of Ag⁺ ions is known to be crucial for initiating and controlling the anisotropic growth of one-dimensional Au nanocrystals such as nanorods, ⁶⁶ while the exact mechanism is yet to be resolved. Three plausible mechanisms have been proposed to account for the role of Ag, ^{1,66} including the facet-specific capping effect of the Ag–bromide complex, ^{31,67} the underpotential deposition of the Ag sub-monolayer on a specific set of facets, ^{10,25,68,69} and the Ag-mediated spherical-to-cylindrical shape conversion for the CTAB micelles that can serve as a soft template. ⁷⁰ In this work, if AgNO₃ was not added into the reaction, the dominant morphology of the Pd–

Au nanocrystals would be nearly spherical (Figure S5). Figure 5 shows the products obtained when a volume of 10 mM AgNO₃ ($V_{\rm Ag}$) was increased from 5 to 20 μ L, or the Ag/Au ratio in the precursor solution ($r_{\rm Ag/Au}$) was increased from 1/16 to 4/16. For the product obtained at $V_{\rm Ag} = 5~\mu$ L (Figure 5a), the anisotropic one-dimensional morphology was still observed, while the Au end was rounded rather than sharpened. As $V_{\rm Ag}$ increased, the length of the Pd–Au nanopyramids increased and the Au end became sharper. At $V_{\rm Ag} = 20~\mu$ L, two- and three-branched growth modes were also observed, accompanied by an increase in length (Figure 5d). These observations indicated that the role played by Ag⁺ ions in promoting the anisotropic growth of Au was highly dependent on its concentration in the growth solution.

The extinction spectra of the products are shown in Figure 5e, while the morphological parameters are statistically plotted in Figure 5f. The product obtained at $V_{Ag} = 5 \mu L$ showed a single plasmon band at 535 nm, implying a very small aspect ratio. The extinction spectrum for the sample obtained at $V_{
m Ag}$ = 10 μ L exhibited a main peak at 556 nm and a shoulder peak at 530 nm. The main peak red-shifted to 575 nm for $V_{\rm Ag}$ = 15 $\mu {\rm L}$, indicating the increase in aspect ratio. At $V_{\rm Ag} = 20~\mu {\rm L}$, the spectrum showed a main peak at 532 nm and a shoulder peak around 650 nm. This spectrum implies that the product yield decreased for the nanocrystals with larger aspect ratios and some nearly spherical or low-aspect-ratio particles were formed, contributing to the main extinction peak at 532 nm. The statistics of morphological parameters in Figure 5f are consistent with the evolution of extinction spectra. The product at $V_{\rm Ag}$ = 5 μL had an average width of 19.3 nm, an average length of 27.6 nm, and an average aspect ratio of 1.44. As the V_{Ag} increased to 10 and 15 μ L, the average width

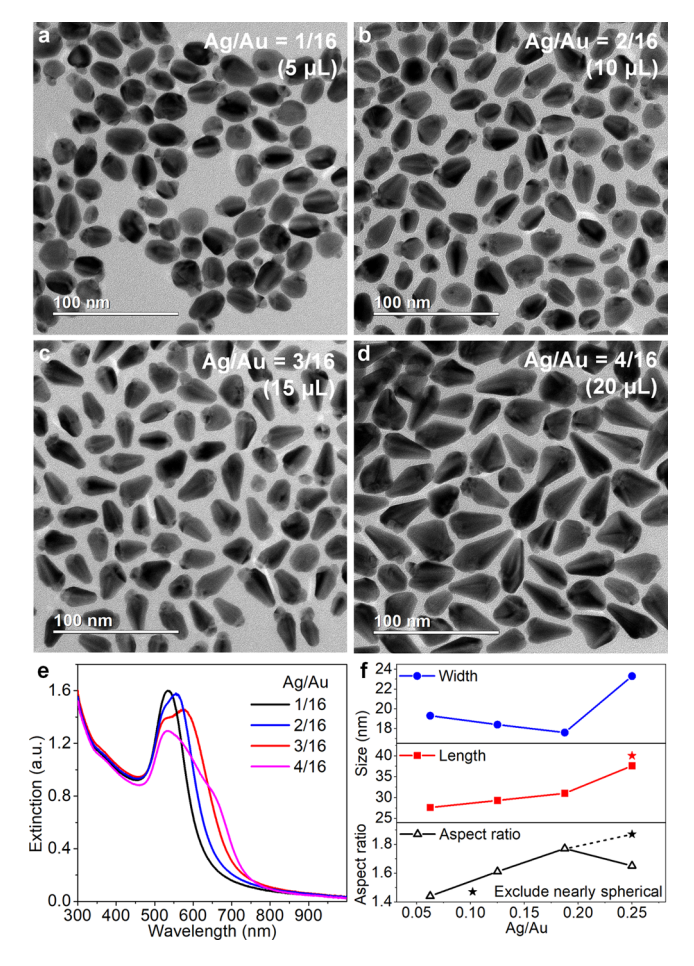


Figure 5. Evolution of morphology and extinction spectra for the Pd–Au nanopyramids synthesized with the addition of different amounts of AgNO₃. (a–d) TEM images of the Pd–Au nanopyramids obtained with the introduction of different volumes of 10 mM AgNO₃ (different Ag/Au ratios in the precursor solution): (a) 5 μ L (1/16), (b) 10 μ L (1/16), (c) 15 μ L (3/16), and (d) 20 μ L (4/16). (e) Evolution of extinction spectra as a function of Ag/Au ratio. (f) Statistical plots of the average width, length, and aspect ratio of the asprepared Pd–Au nanopyramids. The star-shaped points indicate the statistical data excluding the nearly spherical particles.

decreased to 18.4 and 17.6 nm, the average length increased to 29.3 and 31.0 nm, and the average aspect ratio increased to 1.61 and 1.77, respectively. This result indicates the increase of Ag+ ions could promote the longitudinal growth while suppressing the transverse growth. At $V_{\rm Ag}$ = 20 $\mu \rm L$, both the average width (23.3 nm) and average length (37.6 nm) became larger, while the average aspect ratio dropped to 1.65. As the extinction spectrum implies the occurrence of nearly spherical or low-aspect-ratio nanoparticles at $V_{\rm Ag}$ = 20 $\mu {\rm L}$, the average morphological parameters for the whole product could no longer reflect the shape evolution of Pd-Au pyramidal nanocrystals. As such, we excluded the nearly spherical or low-aspect-ratio nanoparticles from the statistics for $V_{\rm Ag}$ = 20 μ L. The modified morphological parameters (plotted as starshaped symbols in Figure 5f) show that the aspect ratio of the Pd—Au nanopyramids further increased as the V_{Ag} increased to 20 μ L, while the width of the nanopyramids also obviously increased. At V_{Ag} = 20 μ L, although the Pd—Au nanopyramids could be further elongated, the extinction spectrum indicates a worsened uniformity for the particles. Another interesting result is that the Au end was sharpened as V_{Ag} was increased. The analysis in Figure S6 indicates that the average tip angle of the Au end was reduced from 41.1 to 29.9° as $V_{\rm Ag}$ increased from 5 to 20 μ L. The Pd—Au nanopyramids with a sharpened Au tip could offer a plasmonic hot spot with large field enhancement and confinement for many tip-enhanced spectroscopies and plasmon-enhanced applications.

Besides tuning the aspect ratio and tip sharpness, the morphology of the Pd-Au nanocrystals can be controlled by varying the amounts of the HAuCl₄ precursor (Figure S7), Pd seeds (Figure S8), and reducing agent (Figure S9). In the case of decreasing the amount of Asc-2P or increasing the amount of Pd seeds, the Pd-Au nanocrystals took a Janus-type heterodimer nanostructure, in which the size of the Au domain was similar to that of the Pd seed (Figures S8b and S9c). These Pd-Au Janus nanocrystals may have interesting properties for optical and catalytic applications. In the case of accelerating the reduction rate by increasing the amount of Asc-2P or using a strong reducing agent such as AA, the faster reduction produced sufficient Au atoms for the nucleation and growth from multiple vertices on the Pd decahedron. Specifically, lateral growth from two, three, four, and five edge vertices of the decahedron are all observed (Figure \$10) for the generation of multiple-armed pentagrams (Figure S11). It is worth noting that the symmetric, five-armed nanocrystals with a pentagram shape have also been synthesized from decahedral seeds for several monometallic and alloy systems. 49-52 However, it has been a major challenge to synthesize asymmetric, multiple-armed nanocrystals with 2-4 branches. The present work suggests that such asymmetric nanocrystals could be obtained by carefully controlling the deposition rate of the atoms and/or with the help of facetspecific capping agents.

When a symmetric nanocrystal is laterally grown from a smaller decahedron, a multiple-armed pentagram is more favorable than a large decahedron due to a crystallographybased reason. The pentagram morphology with lateral overgrowth along five twin boundaries of a decahedron was observed in the synthesis of monometallic and alloy nanocrystals. 49-53 It is well known that a decahedron experiences lattice strain due to the missing of 7.35° in the integration of five tetrahedral units by sharing the {111} plane with an angle of 70.53°, and a large intrinsic strain field of lattice displacement would exist in a decahedron.71-75 When the decahedron grows into larger sizes, the lateral enlargement would lead to an increased lattice strain. As such, faceting, surface reconstruction, and twin interface migration would occur to release the lattice strain energy. Furthermore, the distortion-induced body-centered tetragonal phase was observed in penta-twinned Ag nanowires with an average diameter of 85 nm under ambient conditions.⁷⁹ We observed a large expansive lattice strain in the HAADF-STEM image of a two-branched Pd-Au nanocrystal obtained through lateral growth along two twin boundaries. As shown in Figure 6a, the Pd and Au domains are recognizable due to the contrast, and the two elongated twin boundaries are indicated by red arrows. The penta-twinned structure could be clearly resolved in the bright-field HRTEM (Figure 6b) and inversed FFT images (Figure 6c). The FFT pattern in Figure 6d obtained from the region between the two elongated twin boundaries could be indexed as the diffraction of the fcc lattice along the (110) zone axis, while the interplanar spacings and the interplanar angles were not consistent with the theoretical values of the fcc-Au lattice. As schematically illustrated in Figure 6e, the

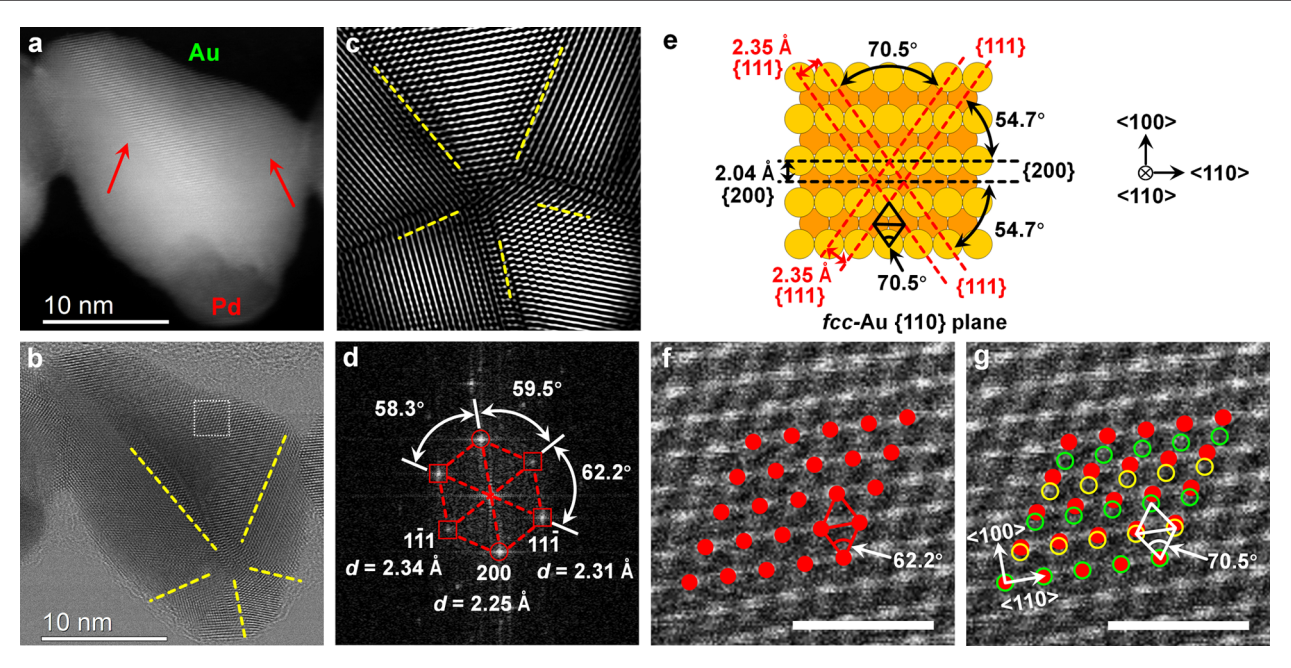


Figure 6. Expansive strain in a two-armed Pd—Au nanocrystal. (a) HAADF-STEM image of a two-armed Pd—Au nanocrystal formed through the lateral growth. The twin boundaries in the two elongated Au arms are indicated by red arrows. (b) Bright-field HRTEM image of the two-armed Pd—Au nanocrystal. The five twin boundaries are indicated by yellow dashed lines. (c) Inversed FFT image of the region near the Pd seed clearly shows the five subunits. (d) FFT pattern of the shared subunits connecting the two elongated Au arms, the region marked by a white box in (b). The pattern is similar to the fcc (110) zone axis, while the interplanar distances and interplanar angles are different from the standard lattice of fcc-Au. (e) Schematic illustration of the {110} planes of fcc-Au. (f, g) Atomic-resolution HRTEM images taken from the white box in (b). The solid red circles indicate the estimated atomic positions in the TEM image. The open green and yellow circles indicate the theoretical atomic positions of the fcc-Au lattice. There is a large displacement between these two lattices, especially for the {200} planes with an expansive strain of 10.3%. The scale bar is 1 nm.

black dashed lines indicate the {200} planes with an interplanar spacing $d_{200}=2.04$ Å, and the red dashed lines indicate the {111} planes with $d_{111}=2.35$ Å. The angle between the {200} and {111} planes is $\theta_{200\wedge111}=54.7^\circ$ and that between the two {111} planes is $\theta_{111\wedge111}=70.5^\circ$. However, the parameters measured in Figure 6d are as follows: $d_{200(\mathrm{m})}=2.25$ Å, $d_{111(\mathrm{m})}=2.31$ and 2.34 Å, $\theta_{200\wedge111(\mathrm{m})}=58.3$ and 59.5° , and $\theta_{111\wedge111(\mathrm{m})}=62.2^\circ$. For the interplanar spacing of the {200} planes, in particular, the measured value of 2.25 Å shows a 10.3% expansion compared with the theoretical value of 2.04 Å, which is larger than the relative expansion of 5% observed in a 17-nm Au decahedron.

The high-resolution HAADF-STEM image with an atomic lattice taken from the white square in Figure 6b is further analyzed in Figure 6f,g. The atomic arrangement with estimated positions (red solid circles) shows a large displacement compared with the theoretical atomic lattice of fcc-Au (green and yellow open circles). Similarly, the measured interplanar angle between the two {111} planes is $\theta_{111\wedge111(m)}$ = 62.2°, which is 11.8% smaller than the theoretical value of 70.5°. When only one twin boundary is elongated for the nanopyramids shown in Figure 2b, the lattice expansive strain for filling the 7.35° gap does not need to exist in this elongated branch. However, in the two-armed Pd-Au nanocrystal, the region connecting the two branches elongated from the twin boundaries of the Pd decahedral seed would experience a large lattice strain. Minimizing the energy of lattice strain may serve as a driving force for forming a multiple-armed pentagram rather than an isotopically enlarged decahedron.

CONCLUSIONS

In summary, we have systematically investigated the formation of Pd-Au nanopyramids from Pd decahedral seeds through site-selected and asymmetric growth. The morphological and structural features make the vertices of the Pd decahedral seeds higher in surface free energy and thus particularly active for the nucleation and deposition of Au. The growth could be conducted at a slow reduction rate by forming the AuBr₄precursor, together with the use of Asc-2P as a relatively weak reducing agent. We observed both the asymmetric lateral growth from one of the edge vertices along the twin boundary and the asymmetric vertical growth from one of the axial vertices along the fivefold axis. In general, lateral growth is more favorable due to the higher activity and larger number of edge vertices. The anisotropic nanopyramids exhibited dual plasmon resonance peaks and the evolution of their extinction spectra could be used to track the growth process. The addition of Ag⁺ ions was found to play a vital role in controlling the aspect ratio and tip sharpness of the nanopyramids. The morphology and size of the Pd-Au nanocrystals could also be controlled by varying the concentrations of the precursor, reducing agent, and seed. The results from this research not only advance our understanding of seed-mediated growth based on multiplytwinned decahedral seeds but also provide a way for the synthesis of anisotropic and asymmetric metal nanocrystals with specific internal structures and optical properties.

■ EXPERIMENTAL SECTION

Materials. Diethylene glycol (DEG, 99.0%, lot no. BCBV7882), poly(vinylpyrrolidone) (PVP, MW ≈ 55 000), sodium sulfate

 (Na_2SO_4) , tetrachloroauric(III) acid $(HAuCl_4)$, silver nitrate $(AgNO_3)$, sodium tetrachloropalladate(II) (Na_2PdCl_4) , hexadecyltrimethylammonium bromide (CTAB), L-ascorbic acid 2-phosphate trisodium salt (Asc-2P), and ascorbic acid (AA) were all purchased from Sigma-Aldrich. Ethylene glycol (EG) was ordered from J.T. Baker. All chemicals were used as received. Deionized water with a resistivity of $18.2\ M\Omega\cdot cm$ was used throughout the experiments.

Synthesis of Pd Decahedral Seeds. $N_{a_2}SO_4$ (176 mg) was added into a 50 mL flask equipped with a stirring bar. Then, 8 mL of DEG-based PVP solution (20 mg/mL) was added. The flask was placed in an oil bath held at 105 °C under stirring (450 rpm). Immediately, 4 mL of DEG-based $N_{a_2}PdCl_4$ (15.5 mg/mL) was added in one shot using a pipet. After 6 h, the synthesis was quenched by immersing the flask in an ice-water bath. The solid products were collected by adding acetone (three times of the reaction solution) and centrifuging at 6000 rpm for 10 min. The precipitate was dispersed in water and centrifuged three times at 16 500 rpm for 25 min. The Pd decahedra were finally dispersed in 4 mL of EG for further use as seeds.

Synthesis of Pd–Au Nanopyramids. In a standard synthesis, 2.45 mL of an aqueous mixture containing 40 μ L of the Pd decahedral seeds, 20 μ L of HAuCl₄ (40 mM), 1 mL of CTAB (200 mM), and 15 μ L of AgNO₃ (10 mM) was first prepared in a 20 mL vial. The mixture showed a deep brown color due to the formation of AuBr₄ (CTA–AuBr₄ complex). Next, 50 μ L of aqueous Asc-2P (100 mM) was added. The mixture turned colorless due to the reduction of AuBr₄ (Au³⁺ to Au⁺). After mixing by gentle shaking, the vial was placed in a water bath held at 37 °C for 3 h. The solid products were collected by centrifugation at 14 000 rpm for 10 min and washed twice with water.

Characterization. The TEM images were taken using a Hitachi HT7700 microscope operated at 120 kV. The HAADF-STEM and EDX mapping images were acquired using a Hitachi HD-2700 STEM microscope. The UV-vis-NIR extinction spectra were recorded on an Agilent Cary 60 spectrometer.

ASSOCIATED CONTENT

5 Supporting Information

The Supporting Information is available free of charge at https://pubs.acs.org/doi/10.1021/acs.chemmater.1c01489.

Schematic illustration and definition of various features on a decahedron, laterally grown Pd—Au nanopyramid, and vertically grown Pd—Au nanopyramids, respectively; TEM image of the Pd decahedral seeds; molecular structures of Asc-2P and AA; schematics of the different growth modes; morphological evolution at different concentrations of AgNO₃; TEM images of Pd—Au nanocrystals obtained when varying the amounts of HAuCl₄, Pd seeds, and Asc-2P, respectively (PDF)

■ AUTHOR INFORMATION

Corresponding Author

Younan Xia — The Wallace H. Coulter Department of Biomedical Engineering, Georgia Institute of Technology and Emory University, Atlanta, Georgia 30332, United States; School of Chemistry and Biochemistry, Georgia Institute of Technology, Atlanta, Georgia 30332, United States; orcid.org/0000-0003-2431-7048; Email: younan.xia@bme.gatech.edu

Authors

Li Zhou – The Wallace H. Coulter Department of Biomedical Engineering, Georgia Institute of Technology and Emory University, Atlanta, Georgia 30332, United States; School of Physics and Technology, Wuhan University, Wuhan, Hubei 430072, P. R. China; Occid.org/0000-0002-7508-6633

Xiaoyu Qiu — The Wallace H. Coulter Department of Biomedical Engineering, Georgia Institute of Technology and Emory University, Atlanta, Georgia 30332, United States; orcid.org/0000-0001-7952-3346

Zhiheng Lyu — School of Chemistry and Biochemistry, Georgia Institute of Technology, Atlanta, Georgia 30332, United States; © orcid.org/0000-0002-1343-4057

Ming Zhao — School of Chemistry and Biochemistry, Georgia Institute of Technology, Atlanta, Georgia 30332, United States; © orcid.org/0000-0003-0127-1470

Complete contact information is available at: https://pubs.acs.org/10.1021/acs.chemmater.1c01489

Author Contributions

L.Z. and X.Q. contributed equally to this work.

Notes

The authors declare no competing financial interest.

■ ACKNOWLEDGMENTS

This work was supported in part by the National Science Foundation (CHE-1804970) and start-up funds from the Georgia Institute of Technology. L.Z. was also partially supported by the National Key R&D Program of China (2017YFA0303402 and 2020YFA0211300), the National Natural Science Foundation of China (11874293), and the Young Talent Training Program of Wuhan University. TEM and STEM images were captured at the Materials Characterization Facilities of the GT's Institute of Electronics and Nanotechnology (IEN), a member of the National Nanotechnology Coordinated Infrastructure (NNCI), and supported by the National Science Foundation (ECCS-1542174).

REFERENCES

- (1) Huo, D.; Kim, M. J.; Lyu, Z. H.; Shi, Y. F.; Wiley, B. J.; Xia, Y. N. One-Dimensional Metal Nanostructures: From Colloidal Syntheses to Applications. *Chem. Rev.* **2019**, *119*, 8972–9073.
- (2) Lim, B.; Xia, Y. N. Metal Nanocrystals with Highly Branched Morphologies. *Angew. Chem., Int. Ed.* **2011**, *50*, 76–85.
- (3) Sau, T. K.; Rogach, A. L. Nonspherical Noble Metal Nanoparticles: Colloid-Chemical Synthesis and Morphology Control. *Adv. Mater.* **2010**, *22*, 1781–1804.
- (4) Link, S.; El-Sayed, M. A. Spectral Properties and Relaxation Dynamics of Surface Plasmon Electronic Oscillations in Gold and Silver Nanodots and Nanorods. *J. Phys. Chem. B* **1999**, 103, 8410–8426
- (5) Murphy, C. J.; San, T. K.; Gole, A. M.; Orendorff, C. J.; Gao, J. X.; Gou, L.; Hunyadi, S. E.; Li, T. Anisotropic Metal Nanoparticles: Synthesis, Assembly, and Optical Applications. *J. Phys. Chem. B* **2005**, *109*, 13857–13870.
- (6) Liu, M. Z.; Guyot-Sionnest, P.; Lee, T. W.; Gray, S. K. Optical Properties of Rodlike and Bipyramidal Gold Nanoparticles from Three-Dimensional Computations. *Phys. Rev. B* **2007**, *76*, No. 235428.
- (7) Chow, T. H.; Li, N. N.; Bai, X. P.; Zhuo, X. L.; Shao, L.; Wang, J. F. Gold Nanobipyramids: An Emerging and Versatile Type of Plasmonic Nanoparticles. *Acc. Chem. Res.* **2019**, *52*, 2136–2146.
- (8) Gilroy, K. D.; Peng, H. C.; Yang, X.; Ruditskiy, A.; Xia, Y. N. Symmetry Breaking during Nanocrystal Growth. *Chem. Commun.* **2017**, 53, 4530–4541.
- (9) Lohse, S. E.; Burrows, N. D.; Scarabelli, L.; Liz-Marzán, L. M.; Murphy, C. J. Anisotropic Noble Metal Nanocrystal Growth: The Role of Halides. *Chem. Mater.* **2014**, *26*, 34–43.
- (10) Walsh, M. J.; Barrow, S. J.; Tong, W. M.; Funston, A. M.; Etheridge, J. Symmetry Breaking and Silver in Gold Nanorod Growth. *ACS Nano* **2015**, *9*, 715–724.

- (11) Elechiguerra, J. L.; Reyes-Gasga, J.; Yacaman, M. J. The Role of Twinning in Shape Evolution of Anisotropic Noble Metal Nanostructures. *J. Mater. Chem.* **2006**, *16*, 3906–3919.
- (12) Shen, X. S.; Wang, G. Z.; Hong, X.; Xie, X.; Zhu, W.; Li, D. P. Anisotropic Growth of One-Dimensional Silver Rod-Needle and Plate-Belt Heteronanostructures Induced by Twins and hcp Phase. *J. Am. Chem. Soc.* **2009**, *131*, 10812–10813.
- (13) Xia, X. H.; Xia, Y. N. Symmetry Breaking during Seeded Growth of Nanocrystals. *Nano Lett.* **2012**, *12*, 6038–6042.
- (14) Zhou, S.; Zhao, M.; Yang, T. H.; Xia, Y. N. Decahedral Nanocrystals of Noble Metals: Synthesis, Characterization, and Applications. *Mater. Today* **2019**, *22*, 108–131.
- (15) Wang, X.; Vara, M.; Luo, M.; Huang, H. W.; Ruditskiy, A.; Park, J.; Bao, S. X.; Liu, J. Y.; Howe, J.; Chi, M. F.; Xie, Z. X.; Xia, Y. N. Pd@Pt Core-Shell Concave Decahedra: A Class of Catalysts for the Oxygen Reduction Reaction with Enhanced Activity and Durability. J. Am. Chem. Soc. 2015, 137, 15036–15042.
- (16) McEachran, M.; Keogh, D.; Pietrobon, B.; Cathcart, N.; Gourevich, I.; Coombs, N.; Kitaev, V. Ultrathin Gold Nanoframes through Surfactant-Free Templating of Faceted Pentagonal Silver Nanoparticles. *J. Am. Chem. Soc.* **2011**, *133*, 8066–8069.
- (17) Fan, N. N.; Yang, Y.; Wang, W. F.; Zhang, L. J.; Chen, W.; Zou, C.; Huang, S. M. Selective Etching Induces Selective Growth and Controlled Formation of Various Platinum Nanostructures by Modifying Seed Surface Free Energy. ACS Nano 2012, 6, 4072–4082.
- (18) Sun, Y. G.; Mayers, B.; Herricks, T.; Xia, Y. N. Polyol Synthesis of Uniform Silver Nanowires: A Plausible Growth Mechanism and the Supporting Evidence. *Nano Lett.* **2003**, *3*, 955–960.
- (19) Koczkur, K. M.; Mourdikoudis, S.; Polavarapu, L.; Skrabalak, S. E. Polyvinylpyrrolidone (PVP) in Nanoparticle Synthesis. *Dalton Trans.* **2015**, *44*, 17883–17905.
- (20) Pietrobon, B.; McEachran, M.; Kitaev, V. Synthesis of Size-Controlled Faceted Pentagonal Silver Nanorrods with Tunable Plasmonic Properties and Self-Assembly of These Nanorods. *ACS Nano* **2009**, *3*, 21–26.
- (21) Murshid, N.; Kitaev, V. Role of Poly(vinylpyrrolidone) (PVP) and other Sterically Protecting Polymers in Selective Stabilization of {111} and {100} Facets in Pentagonally Twinned Silver Nanoparticles. *Chem. Commun.* **2014**, *50*, 1247–1249.
- (22) Murshid, N.; Keogh, D.; Kitaev, V. Optimized Synthetic Protocols for Preparation of Versatile Plasmonic Platform Based on Silver Nanoparticles with Pentagonal Symmetries. *Part. Part. Syst. Charact.* **2014**, *31*, 178–189.
- (23) Lofton, C.; Sigmund, W. Mechanisms Controlling Crystal Habits of Gold and Silver Colloids. *Adv. Funct. Mater.* **2005**, *15*, 1197–1208.
- (24) Zhang, S. H.; Jiang, Z. Y.; Xie, Z. X.; Xu, X.; Huang, R. B.; Zheng, L. S. Growth of Silver Nanowires from Solutions: A Cyclic Penta-Twinned-Crystal Growth Mechanism. *J. Phys. Chem. B* **2005**, 109, 9416–9421.
- (25) Liu, M. Z.; Guyot-Sionnest, P. Mechanism of Silver(I)-Assisted Growth of Gold Nanorods and Bipyramids. *J. Phys. Chem. B* **2005**, 109, 22192–22200.
- (26) Jin, M. S.; He, G. N.; Zhang, H.; Zeng, J.; Xie, Z. X.; Xia, Y. N. Shape-Controlled Synthesis of Copper Nanocrystals in an Aqueous Solution with Glucose as a Reducing Agent and Hexadecylamine as a Capping Agent. *Angew. Chem., Int. Ed.* **2011**, *50*, 10560–10564.
- (27) Yoon, J.; Khi, N. T.; Kim, H.; Kim, B.; Baik, H.; Back, S.; Lee, S.; Lee, S. W.; Kwon, S. J.; Lee, K. High Yield Synthesis of Catalytically Active Five-Fold Twinned Pt Nanorods from a Surfactant-Ligated Precursor. *Chem. Commun.* **2013**, *49*, 573–575.
- (28) Huang, H. W.; Ruditskiy, A.; Choi, S. I.; Zhang, L.; Liu, J. Y.; Ye, Z. Z.; Xia, Y. N. One-Pot Synthesis of Penta-twinned Palladium Nanowires and Their Enhanced Electrocatalytic Properties. *ACS Appl. Mater. Interfaces* **2017**, *9*, 31203–31212.
- (29) Zheng, Y.; Tao, J.; Liu, H.; Zeng, J.; Yu, T.; Ma, Y.; Moran, C.; Wu, L.; Zhu, Y.; Liu, J.; Xia, Y. Facile Synthesis of Gold Nanorice Enclosed by High-Index Facets and Its Application for CO Oxidation. *Small* **2011**, *7*, 2307–2312.

- (30) Zhang, X.; Tsuji, M.; Lim, S.; Miyamae, N.; Nishio, M.; Hikino, S.; Umezu, M. Synthesis and Growth Mechanism of Pentagonal Bipyramid-Shaped Gold-Rich Au/Ag Alloy Nanoparticles. *Langmuir* **2007**, 23, 6372–6376.
- (31) Sánchez-Iglesias, A.; Winckelmans, N.; Altantzis, T.; Bals, S.; Grzelczak, M.; Liz-Marzán, L. M. High-Yield Seeded Growth of Monodisperse Pentatwinned Gold Nanoparticles through Thermally Induced Seed Twinning. *J. Am. Chem. Soc.* **2017**, *139*, 107–110.
- (32) Kou, X.; Ni, W.; Tsung, C. K.; Chan, K.; Lin, H. Q.; Stucky, G. D.; Wang, J. Growth of Gold Bipyramids with Improved Yield and Their Curvature-Directed Oxidation. *Small* **2007**, *3*, 2103–2113.
- (33) Kou, X.; Zhang, S.; Tsung, C. K.; Yeung, M. H.; Shi, Q.; Stucky, G. D.; Sun, L.; Wang, J.; Yan, C. Growth of Gold Nanorods and Bipyramids using CTEAB Surfactant. *J. Phys. Chem. B* **2006**, *110*, 16377–16383.
- (34) Yoo, H.; Jang, M. H. Size-Controlled Synthesis of Gold Bipyramids using an Aqueous Mixture of CTAC and Salicylate Anions as the Soft Template. *Nanoscale* **2013**, *5*, 6708–6712.
- (35) Kang, X.; Ruan, Q.; Zhang, H.; Bao, F.; Guo, J.; Tang, M.; Cheng, S.; Wang, J. Concave Gold Bipyramids Bound with Multiple High-Index Facets: Improved Raman and Catalytic Activities. *Nanoscale* **2017**, *9*, 5879–5886.
- (36) Li, Q.; Zhuo, X.; Li, S.; Ruan, Q.; Xu, Q.; Wang, J. Production of Monodisperse Gold Nanobipyramids with Number Percentages Approaching 100% and Evaluation of Their Plasmonic Properties. *Adv. Opt. Mater.* **2015**, 3, 801–812.
- (37) Zhang, J.; Langille, M. R.; Mirkin, C. A. Synthesis of Silver Nanorods by Low Energy Excitation of Spherical Plasmonic Seeds. *Nano Lett.* **2011**, *11*, 2495–2498.
- (38) Zhou, G. J.; Yang, Y.; Han, S. H.; Chen, W.; Fu, Y. Z.; Zou, C.; Zhang, L. J.; Huang, S. M. Growth of Nanobipyramid by Using Large Sized Au Decahedra as Seeds. *ACS Appl. Mater. Interfaces* **2013**, *5*, 13340–13352.
- (39) Li, X. L.; Yang, Y.; Zhou, G. J.; Han, S. H.; Wang, W. F.; Zhang, L. J.; Chen, W.; Zou, C.; Huang, S. M. The Unusual Effect of AgNO₃ on the Growth of Au Nanostructures and Their Catalytic Performance. *Nanoscale* **2013**, *5*, 4976–4985.
- (40) Huang, H. W.; Zhang, L.; Lv, T.; Ruditskiy, A.; Liu, J. Y.; Ye, Z. Z.; Xia, Y. N. Five-Fold Twinned Pd Nanorods and Their Use as Templates for the Synthesis of Bimetallic or Hollow Nanostructures. *ChemNanoMat* **2015**, *1*, 246–252.
- (41) Ruditskiy, A.; Vara, M.; Huang, H.; Xia, Y. N. Oxidative Etching of Pd Decahedral Nanocrystals with a Penta-twinned Structure and Its Impact on Their Growth Behavior. *Chem. Mater.* **2017**, 29, 5394–5400.
- (42) Seo, D.; Yoo, C., Il; Jung, J.; Song, H. Ag-Au-Ag Heterometallic Nanorods Formed through Directed Anisotropic Growth. *J. Am. Chem. Soc.* **2008**, *130*, 2940–2941.
- (43) Xu, L.; Wang, K.; Jiang, B.; Chen, W.; Liu, F. Y.; Hao, H.; Zou, C.; Yang, Y.; Huang, S. M. Competitive Effect in The Growth of Pd-Au-Pd Segmental Nanorods. *Chem. Mater.* **2016**, 28, 7394–7403.
- (44) Luo, M.; Huang, H. W.; Choi, S. I.; Zhang, C.; da Silva, R. R.; Peng, H. C.; Li, Z. Y.; Liu, J. Y.; He, Z. K.; Xia, Y. N. Facile Synthesis of Ag Nanorods with No Plasmon Resonance Peak in the Visible Region by Using Pd Decahedra of 16 nm in Size as Seeds. *ACS Nano* **2015**, *9*, 10523–10532.
- (45) Zhou, L.; Lyu, Z.; Xia, Y. Pencil-Like Ag Nanorods Asymmetrically Capped by Pd. Chem. Mater. 2020, 32, 5361-5367.
- (46) Luo, M.; Ruditskiy, A.; Peng, H. C.; Tao, J.; Figueroa-Cosme, L.; He, Z. K.; Xia, Y. N. Penta-Twinned Copper Nanorods: Facile Synthesis via Seed-Mediated Growth and Their Tunable Plasmonic Properties. *Adv. Funct. Mater.* **2016**, *26*, 1209–1216.
- (47) Langille, M. R.; Zhang, J.; Mirkin, C. A. Plasmon-Mediated Synthesis of Heterometallic Nanorods and Icosahedra. *Angew. Chem., Int. Ed.* **2011**, *50*, 3543–3547.
- (48) Yang, Y.; Wang, W. F.; Li, X. L.; Chen, W.; Fan, N. N.; Zou, C.; Chen, X.; Xu, X. J.; Zhang, L. J.; Huang, S. M. Controlled Growth of Ag/Au Bimetallic Nanorods through Kinetics Control. *Chem. Mater.* **2013**, 25, 34–41.

- (49) Zhang, H.; Xia, X. H.; Li, W. Y.; Zeng, J.; Dai, Y. Q.; Yang, D. R.; Xia, Y. N. Facile Synthesis of Five-fold Twinned, Starfish-like Rhodium Nanocrystals by Eliminating Oxidative Etching with a Chloride-Free Precursor. *Angew. Chem., Int. Ed.* **2010**, 49, 5296–5300.
- (50) He, R.; Wang, Y. C.; Wang, X. Y.; Wang, Z. T.; Liu, G.; Zhou, W.; Wen, L. P.; Li, Q. X.; Wang, X. P.; Chen, X. Y.; Zeng, J.; Hou, J. G. Facile Synthesis of Pentacle Gold-Copper Alloy Nanocrystals and Their Plasmonic and Catalytic Properties. *Nat. Commun.* **2014**, *5*, No. 4327.
- (51) Cathcart, N.; Coombs, N.; Gourevich, I.; Kitaev, V. Synthesis and Sensing Properties of D-5h Pentagonal Silver Star Nanoparticles. *Nanoscale* **2016**, *8*, 18282–18290.
- (52) Khi, N. T.; Baik, H.; Lee, H.; Yoon, J.; Sohn, J. H.; Lee, K. Rationally Synthesized Five-Fold Twinned Core-Shell Pt₃Ni@Rh Nanopentagons, Nanostars and Nanopaddlewheels for Selective Reduction of a Phenyl Ring of Phthalimide. *Nanoscale* **2014**, *6*, 11007–11012.
- (53) Bazán-Díaz, L.; Mendoza-Cruz, R.; Velázquez-Salazar, J. J.; Plascencia-Villa, G.; Romeu, D.; Reyes-Gasga, J.; Herrera-Becerra, R.; José-Yacamán, M.; Guisbiers, G. Gold-Copper Nanostars as Photothermal Agents: Synthesis and Advanced Electron Microscopy Characterization. *Nanoscale* **2015**, *7*, 20734–20742.
- (54) Velázquez-Salazar, J. J.; Bazán-Díaz, L.; Zhan, Q. F.; Mendoza-Cruz, R.; Montaño-Priede, L.; Guisbiers, G.; Large, N.; Link, S.; José-Yacamán, M. Controlled Overgrowth of Five-Fold Concave Nanoparticles into Plasmonic Nanostars and Their Single-Particle Scattering Properties. ACS Nano 2019, 13, 10113—10128.
- (55) Zhang, L. F.; Zhong, S. L.; Xu, A. W. Highly Branched Concave Au/Pd Bimetallic Nanocrystals with Superior Electrocatalytic Activity and Highly Efficient SERS Enhancement. *Angew. Chem., Int. Ed.* **2013**, 52, 645–649.
- (56) Wu, H. L.; Chen, C. H.; Huang, M. H. Seed-Mediated Synthesis of Branched Gold Nanocrystals Derived from the Side Growth of Pentagonal Bipyramids and the Formation of Gold Nanostars. *Chem. Mater.* **2009**, *21*, 110–114.
- (57) Yang, T. H.; Gilroy, K. D.; Xia, Y. N. Reduction Rate as a Quantitative Knob for Achieving Deterministic Synthesis of Colloidal Metal Nanocrystals. *Chem. Sci.* **2017**, *8*, 6730–6749.
- (58) Huo, D.; Cao, Z.; Li, J.; Xie, M.; Tao, J.; Xia, Y. Seed-Mediated Growth of Au Nanospheres into Hexagonal Stars and the Emergence of a Hexagonal Close-Packed Phase. *Nano Lett.* **2019**, *19*, 3115–3121.
- (59) Huang, H.; Wang, Y.; Ruditskiy, A.; Peng, H.-C.; Zhao, X.; Zhang, L.; Liu, J.; Ye, Z.; Xia, Y. Polyol Syntheses of Palladium Decahedra and Icosahedra as Pure Samples by Maneuvering the Reaction Kinetics with Additives. *ACS Nano* **2014**, *8*, 7041–7050.
- (60) Ruditskiy, A.; Zhao, M.; Gilroy, K. D.; Vara, M.; Xia, Y. Toward a Quantitative Understanding of the Sulfate-Mediated Synthesis of Pd Decahedral Nanocrystals with High Conversion and Morphology Yields. *Chem. Mater.* **2016**, 28, 8800–8806.
- (61) Bard, A. J.; Parsons, R.; Jordan, J. Standard Potentials in Aqueous Solution; Marcel Dekker: New York, 1985; pp 313-320.
- (62) Bai, T.; Tan, Y.; Zou, J.; Nie, M.; Guo, Z.; Lu, X.; Gu, N. AuBr²⁻-Engaged Galvanic Replacement for Citrate-Capped Au–Ag Alloy Nanostructures and Their Solution-Based Surface-Enhanced Raman Scattering Activity. *J. Phys. Chem. B* **2015**, *119*, 28597–28604.
- (63) Yang, T. H.; Peng, H. C.; Zhou, S.; Lee, C. T.; Bao, S. X.; Lee, Y. H.; Wu, J. M.; Xia, Y. N. Toward a Quantitative Understanding of the Reduction Pathways of a Salt Precursor in the Synthesis of Metal Nanocrystals. *Nano Lett.* **2017**, *17*, 334–340.
- (64) Pérez-Juste, J.; Liz-Marzán, L. M.; Carnie, S.; Chan, D. Y. C.; Mulvaney, P. Electric-Field-Directed Growth of Gold Nanorods in Aqueous Surfactant Solutions. *Adv. Funct. Mater.* **2004**, *14*, 571–579.
- (65) Zhu, X.; Yip, H. K.; Zhuo, X.; Jiang, R.; Chen, J.; Zhu, X.; Yang, Z.; Wang, J. Realization of Red Plasmon Shifts up to ~900 nm by AgPd-Tipping Elongated Au Nanocrystals. *J. Am. Chem. Soc.* **2017**, 139, 13837—13846.

- (66) Lohse, S. E.; Murphy, C. J. The Quest for Shape Control: A History of Gold Nanorod Synthesis. *Chem. Mater.* **2013**, 25, 1250–1261.
- (67) Niidome, Y.; Nakamura, Y.; Honda, K.; Akiyama, Y.; Nishioka, K.; Kawasaki, H.; Nakashima, N. Characterization of Silver Ions Adsorbed on Gold Nanorods: Surface Analysis by using Surface-Assisted Laser Desorption/Ionization Time-of-Flight Mass Spectrometry. *Chem. Commun.* **2009**, 1754–1756.
- (68) Orendorff, C. J.; Murphy, C. J. Quantitation of Metal Content in the Silver-Assisted Growth of Gold Nanorods. *J. Phys. Chem. B* **2006**, *110*, 3990–3994.
- (69) Placido, T.; Comparelli, R.; Giannici, F.; Cozzoli, P. D.; Capitani, G.; Striccoli, M.; Agostiano, A.; Curri, M. L. Photochemical Synthesis of Water-Soluble Gold Nanorods: the Role of Silver in Assisting Anisotropic Growth. *Chem. Mater.* **2009**, *21*, 4192–4202.
- (70) Jackson, S. R.; McBride, J. R.; Rosenthal, S. J.; Wright, D. W. Where's the Silver? Imaging Trace Silver Coverage on the Surface of Gold Nanorods. *J. Am. Chem. Soc.* **2014**, *136*, 5261–5263.
- (71) Johnson, C. L.; Snoeck, E.; Ezcurdia, M.; Rodríguez-González, B.; Pastoriza-Santos, I.; Liz-Marzán, L. M.; Hÿtch, M. J. Effects of Elastic Anisotropy on Strain Distributions in Decahedral Gold Nanoparticles. *Nat. Mater.* **2008**, *7*, 120–124.
- (72) Chen, C. C.; Zhu, C.; White, E. R.; Chiu, C. Y.; Scott, M. C.; Regan, B. C.; Marks, L. D.; Huang, Y.; Miao, J. W. Three-Dimensional Imaging of Dislocations in a Nanoparticle at Atomic Resolution. *Nature* **2013**, 496, 74–77.
- (73) Goris, B.; De Beenhouwer, J.; De Backer, A.; Zanaga, D.; Batenburg, K. J.; Sánchez-Iglesias, A.; Liz-Marzán, L. M.; Van Aert, S.; Bals, S.; Sijbers, J.; Tendeloo, G. Measuring Lattice Strain in Three Dimensions through Electron Microscopy. *Nano Lett.* **2015**, *15*, 6996–7001.
- (74) Walsh, M. J.; Yoshida, K.; Kuwabara, A.; Pay, M. L.; Gai, P. L.; Boyes, E. D. On the Structural Origin of the Catalytic Properties of Inherently Strained Ultrasmall Decahedral Gold Nanoparticles. *Nano Lett.* **2012**, *12*, 2027–2031.
- (75) Nilsson Pingel, T.; Jørgensen, M.; Yankovich, A. B.; Grönbeck, H.; Olsson, E. Influence of Atomic Site-Specific Strain on Catalytic Activity of Supported Nanoparticles. *Nat. Commun.* **2018**, *9*, No. 2722.
- (76) Casillas, G.; Velázquez-Salazar, J. J.; José-Yacamán, M. A New Mechanism of Stabilization of Large Decahedral Nanoparticles. *J. Phys. Chem. C* **2012**, *116*, 8844–8848.
- (77) Song, M.; Wu, Z. G.; Lu, N.; Li, D. S. Strain Relaxation-Induced Twin Interface Migration and Morphology Evolution of Silver Nanoparticles. *Chem. Mater.* **2019**, *31*, 842–850.
- (78) Patala, S.; Marks, L. D.; de la Cruz, M. O. Elastic Strain Energy Effects in Faceted Decahedral Nanoparticles. *J. Phys. Chem. C* **2013**, 117, 1485–1494.
- (79) Sun, Y. G.; Ren, Y.; Liu, Y. Z.; Wen, J. G.; Okasinski, J. S.; Miller, D. J. Ambient-Stable Tetragonal Phase in Silver Nanostructures. *Nat. Commun.* **2012**, *3*, No. 971.